

Constraining ultralight vector dark matter with the Parkes Pulsar Timing Array second data release

Yu-Mei Wu,^{1,2,3,*} Zu-Cheng Chen,^{4,5,†} Qing-Guo Huang,^{1,3,2,‡} Xingjiang Zhu,^{5,§} N. D. Ramesh Bhat,⁶ Yi Feng,⁷ George Hobbs,⁸ Richard N. Manchester,⁸ Christopher J. Russell,⁹ and R. M. Shannon^{10,11}

¹*School of Fundamental Physics and Mathematical Sciences,*

Hangzhou Institute for Advanced Study, UCAS, Hangzhou 310024, China

²*School of Physical Sciences, University of Chinese Academy of Sciences, No. 19A Yuquan Road, Beijing 100049, China*

³*CAS Key Laboratory of Theoretical Physics, Institute of Theoretical Physics,*

Chinese Academy of Sciences, Beijing 100190, China

⁴*Department of Astronomy, Beijing Normal University, Beijing 100875, China*

⁵*Advanced Institute of Natural Sciences, Beijing Normal University, Zhuhai 519087, China*

⁶*International Centre for Radio Astronomy Research, Curtin University, Bentley, WA 6102, Australia*

⁷*Research Center for Intelligent Computing Platforms, Zhejiang Laboratory, Hangzhou 311100, China*

⁸*Australia Telescope National Facility, CSIRO Astronomy and Space Science, P.O. Box 76, Epping, NSW 1710, Australia*

⁹*CSIRO Scientific Computing, Australian Technology Park,*

Locked Bag 9013, Alexandria, NSW 1435, Australia

¹⁰*Centre for Astrophysics and Supercomputing, Swinburne University of Technology, Hawthorn, VIC, 3122 Australia*

¹¹*Australian Research Council Centre of Excellence in Gravitational Wave Discovery (OzGrav)*

Composed of ultralight bosons, fuzzy dark matter provides an intriguing solution to challenges that the standard cold dark matter model encounters on sub-galactic scales. The ultralight dark matter with mass $m \sim 10^{-23}$ eV will induce a periodic oscillation in gravitational potentials with a frequency in the nanohertz band, leading to observable effects in the arrival times of radio pulses from pulsars. Unlike scalar dark matter, pulsar timing signals induced by the vector dark matter are dependent on the oscillation direction of the vector fields. In this work, we search for ultralight vector dark matter in the mass range of $[2 \times 10^{-24}, 2 \times 10^{-22}]$ eV through its gravitational effect in the Parkes Pulsar Timing Array (PPTA) second data release. Since no statistically significant detection is made, we place 95% upper limits on the local dark matter density as $\rho_{\text{VF}} \lesssim 5 \text{ GeV/cm}^3$ for $m \lesssim 10^{-23}$ eV. As no preferred direction is found for the vector dark matter, these constraints are comparable to those given by the scalar dark matter search with an earlier 12-year data set of PPTA.

I. INTRODUCTION

Numerous astrophysical observations, such as galaxy rotational curves [1, 2], velocity dispersions [3], and gravitational lensing [4] reveal the existence of invisible matter, the so-called dark matter. In combination with observational evidence of the Universe’s accelerating expansion, the standard Lambda Cold Dark Matter (Λ CDM) cosmological model has been established. Precision analyses of the cosmic microwave background show that dark matter constitutes 26% of the total energy density of the present-day universe [5].

The cold dark matter paradigm has achieved great success in describing the structure of galaxies on large scales [6–8], but it is met with puzzling discrepancies between the predictions and observations of galaxies and their clustering on small scales. For example, the N-body simulations based on the cold dark matter model show a much steeper central density profile in the dark matter halos than that inferred from the galaxy rotational

curves (the “core-cusp problem” [9, 10]). The predicted number of subhalos with decreasing mass grows much more steeply than what is observed around galaxies (the “missing-satellites problem” [11, 12]).

Because of the difficulty in solving the small-scale problems as well as the null result in searching for traditional cold dark matter candidates, e.g., weakly interactive massive particles [13], alternative paradigms for dark matter have been proposed. These include the warm dark matter [14] and fuzzy dark matter [15].

The term “fuzzy dark matter” often refers to ultralight scalar particles with a mass around $m \sim 10^{-22}$ eV. Such a dark matter scenario can get the correct relic abundance through the misalignment mechanism similar to that of axions [16]; that is, when the initial value of the scalar field is away from its potential minimum, the field is condensed during inflation when its mass is smaller than the Hubble scale, and then starts a coherent oscillation as a non-relativistic matter at a later epoch. Fuzzy dark matter makes the same large-scale structure predictions as Λ CDM, but the particle’s large de Broglie wavelength, $\lambda \sim \text{kpc}$, suppresses the structure on small scales and thus explains well the corresponding smaller-scale observational phenomena [17].

Besides the scalar particle, a naturally light vector boson predicted in string-inspired models with compactified extra dimensions [18] can also act as a good fuzzy dark

* wuyumei@itp.ac.cn

† Corresponding author: zucheng.chen@bnu.edu.cn

‡ Corresponding author: huangqg@itp.ac.cn

§ Corresponding author: zhuxj@bnu.edu.cn

matter candidate. There are several mechanisms to produce vector dark matter with the correct relic abundance, such as the misalignment mechanism [19, 20], quantum fluctuations during inflation [21, 22], and decay of a network of global cosmic strings [23]. Because of their different spins, if the dark matter is assumed to have interaction with Standard Model, scalar and vector fields couple with Standard Model particles in ways which lead to different observable phenomena. For example, if the vector dark matter particle is a $U(1)_B$ (“ B ” refers to baryon) or $U(1)_{B-L}$ (“ L ” refers to lepton) gauge boson, the so-called “dark photon” would interact with ordinary matter [24], then it can be detected with gravitational-wave interferometers because it exerts forces on test masses and results in displacements [25, 26]; it can also be detected with binary pulsar systems via its effects on the secular dynamics of binary systems [27, 28]. Such a gauge effect is not applicable to scalar dark matter [29].

In addition to unknown interaction with the Standard Model, pure gravitational effects of fuzzy dark matter can also lead to observable results and help distinguish the scalar and vector dark matter. The dark matter field with ultralight mass has a wave nature with the oscillating frequency of $f_{\text{dm}} = mc^2/h = 2.4 \times 10^{-9} (mc^2/10^{-23}\text{eV}) \text{ Hz}$. Such a coherently oscillating field leads to periodic oscillations in the gravitational potentials and further induces periodic signals with the frequency on the order of nanohertz [22, 30], which falls into the sensitive range of the pulsar timing arrays (PTAs). A PTA consists of stable millisecond pulsars for which times of arrival (ToAs) of radio pulses are monitored with high precision over a course of years to decades [31–33]. Any unmodelled signal will induce timing residues, which represent the difference between the measured and predicted ToAs.

In contrast to the ultralight scalar dark matter, the timing residuals caused by the ultralight vector dark matter are dependent on the oscillation direction of the vector fields [22, 30]. Several previous works have used PTA data to search for ultralight scalar dark matter [34–36]. In a recent work [37], a search was performed for the dark photon dark matter in the PPTA second data release (DR2) based on the gauge effect. This resulted in upper limits on the coupling strength between dark photons and ordinary matter, assuming that all dark matter is composed of ultralight dark photons. In this work, we search for ultralight vector dark matter in the mass range of $[2 \times 10^{-24}, 2 \times 10^{-22}] \text{ eV}$ in the PPTA DR2 data set based on the gravitational effect without assuming its interaction with Standard Model particles.

This paper is organized as follows. In Sec. II we describe the observable pulsar timing effects induced by vector dark matter. In Sec. III we provide details of our data analysis. We present the results and conclusions in Sec. IV. In the following sections, we set $c = \hbar = 1$.

II. GRAVITATIONAL EFFECT FROM VECTOR DARK MATTER

In this section, we first introduce the timing residuals caused by the gravitational effect from the ultralight vector dark matter in the Galaxy; a more detailed derivation can be found in Ref. [22].

Assuming no coupling between the ultralight particles and any other fields, we take the action for a free vector field A_μ with mass m as,

$$S = \int d^4x \sqrt{-g} \left(-\frac{1}{4} F^{\mu\nu} F_{\mu\nu} - \frac{1}{2} m^2 A_\mu A^\mu \right), \quad (1)$$

where g is the determinant of the metric $g_{\mu\nu}$ and $F_{\mu\nu} = \partial_\mu A_\nu - \partial_\nu A_\mu$. On Galactic scales, the cosmic expansion is negligible and the background is approximately Minkowski. The energy-momentum tensor carried by the vector dark matter induces perturbations into the metric which, in the Newtonian gauge, can be written as

$$ds^2 = \eta_{\mu\nu} dx^\mu dx^\nu - 2\Phi(t, \mathbf{x}) dt^2 + 2\Psi(t, \mathbf{x}) \delta_{ij} dx^i dx^j + h_{ij}(t, \mathbf{x}) dx^i dx^j, \quad (2)$$

where $\eta_{\mu\nu} = \text{diag}(-1, +1, +1, +1)$ is the background Minkowski metric, Φ and Ψ are gravitational potentials, and h_{ij} describes the traceless spatial metric perturbations. h_{ij} is absent in the scalar-field case and demonstrates the anisotropy induced by additional degrees of freedom in vector fields.

With a huge occupation number, the vector field can be described as a classical wave with a monochromatic frequency determined by its mass. This is a good approximation because the characteristic speed of the dark matter is non-relativistic $v \sim 10^{-3}$. During inflation, only the longitudinal mode of the vector fields survives [21], so the equation of motion of the vector field is given by the component in the oscillating direction $\hat{k} = (\sin \theta \cos \phi, \sin \theta \sin \phi, \cos \theta)$,

$$A_{\hat{k}}(t, \mathbf{x}) = A(\mathbf{x}) \cos(mt + \alpha(\mathbf{x})). \quad (3)$$

The vector fields contribute a time-independent energy density

$$\rho_{\text{VF}}(x) = \frac{1}{2} m^2 A^2(x), \quad (4)$$

and an anisotropic oscillating pressure which leads to oscillating gravitational potentials. By solving the photon geodesic equation from the pulsar to the Earth under the metric Eq. (2), it is found that the metric perturbations that give rise to the observable effects in PTAs are from the spatial components (see the Appendix of [22]). Furthermore, splitting the potential Ψ into a dominant time-independent part and an oscillating part and solving the linear Einstein equation by neglecting the spatial gradient of the oscillating part (which is suppressed by

order of $v \sim 10^{-3}$), the spatial perturbations take the following form,

$$\begin{aligned}\Psi(t, \mathbf{x}) &= \Psi_0(\mathbf{x}) + \Psi_{\text{osc}}(\mathbf{x}) \cos(2mt + 2\alpha(\mathbf{x})), \\ h_{ij}(t, \mathbf{x}) &= h_{\text{osc}}(\mathbf{x}) \cos(2mt + 2\alpha(\mathbf{x})) (\hat{l} \otimes \hat{l} + \hat{n} \otimes \hat{n} - 2\hat{k} \otimes \hat{k}),\end{aligned}\quad (5)$$

where $\Psi_0(x)$ is the potential independent of time determined by the local energy density of the vector field dark matter $\rho_{\text{VF}}(x)$, and \hat{l} and \hat{n} are the unit vectors perpendicular to the propagation direction given by $\hat{l} = (\sin \phi, -\cos \phi, 0)$ and $\hat{n} = (\cos \theta \cos \phi, \cos \theta \sin \phi, -\sin \theta)$, respectively. The amplitudes of potentials in the oscillation part can also be related to $\rho_{\text{VF}}(x)$ through the relationship between $A(x)$ with $\rho_{\text{VF}}(x)$ (Eq. (4)),

$$\begin{aligned}\Psi_{\text{osc}}(\mathbf{x}) &= -\frac{\pi G \rho_{\text{VF}}(\mathbf{x})}{3m^2} \\ &= -2.2 \times 10^{-16} \frac{\rho_{\text{VF}}(\mathbf{x})}{\rho_0} \left(\frac{10^{-23} \text{eV}}{m} \right)^2,\end{aligned}\quad (7)$$

$$\begin{aligned}h_{\text{osc}}(\mathbf{x}) &= \frac{8\pi G \rho_{\text{VF}}(\mathbf{x})}{3m^2} \\ &= 1.7 \times 10^{-15} \frac{\rho_{\text{VF}}(\mathbf{x})}{\rho_0} \left(\frac{10^{-23} \text{eV}}{m} \right)^2.\end{aligned}\quad (8)$$

where we use the measured local energy density $\rho_0 = 0.4 \text{ GeV/cm}^3$ [38] as the normalized factor, and the oscillation frequency in potentials is given by:

$$f = \frac{2m}{2\pi} = 4.8 \times 10^{-9} \text{ Hz} \left(\frac{m}{10^{-23} \text{eV}} \right). \quad (9)$$

The oscillating part of spatial metric Ψ and h_{ij} induces a measurable redshift in the radio pulse propagating from a pulsar to the Earth

$$\begin{aligned}z_{\Psi}(t) &= \Psi_{\text{osc}}(\mathbf{x}_e) \cos(2mt + 2\alpha(\mathbf{x}_e)) \\ &\quad - \Psi_{\text{osc}}(\mathbf{x}_p) \cos[2m(t - |\mathbf{x}_p|) + 2\alpha(\mathbf{x}_p)],\end{aligned}\quad (10)$$

$$z_h(t) = \frac{1}{2} \hat{p}^i \hat{p}^j [h_{ij}(t, \mathbf{x}_e) - h_{ij}(t - |\mathbf{x}_p|, \mathbf{x}_p)], \quad (11)$$

where \mathbf{x}_e and \mathbf{x}_p respectively represent the location of the Earth and the pulsar, and \hat{p} is the unit vector pointing to the pulsar. As the distance between most pulsars and the Earth is at the order of $\mathcal{O}(\text{kpc})$, which is comparable to the de Broglie wavelength of the dark matter, it is legitimate to assume that they are in a region where the vector dark matter keeps its coherent oscillation direction, and that the Earth term and the pulsar term take the same amplitudes Ψ_{osc} and h_{osc} .

Integrating the redshifts separately, the results combine into the total timing residuals,

$$\begin{aligned}R_t &= R_{\Psi} + R_h \\ &= \frac{h_{\text{osc}}}{\pi f} \left\{ \frac{1}{2} \left[(\hat{p} \cdot \hat{l})^2 + (\hat{p} \cdot \hat{n})^2 - 2(\hat{p} \cdot \hat{k})^2 \right] - \frac{1}{8} \right\} \\ &\quad \times \sin(\alpha_e - \alpha_p) \cos(2\pi f t + \alpha_e + \alpha_p),\end{aligned}\quad (12)$$

where we have defined the phases in Earth term and pulsar term as $\alpha_e = \alpha(\mathbf{x}_e)$ and $\alpha_p = \alpha(\mathbf{x}_p) - m|\mathbf{x}_p|$, respectively. Eq. (12) shows that timing residuals induced by

the coherent oscillation of vector dark matter is angle dependent, which is a distinctive feature in comparison to the scalar dark matter; see Ref. [22] for a more detailed comparison.

III. DATA ANALYSIS

Now we turn to search for ultralight vector dark matter in the PPTA DR2 data set, which includes observations for 26 pulsars with a timespan up to 15 years. By balancing sensitivity and computational costs, we choose the six best pulsars, i.e., those with relatively long observational timespan and high timing precision in the array. A summary of the basic properties of these six pulsars is given in Table I.

TABLE I. Basic properties of the 6 pulsars used in our analysis. RMS – the weighted root-mean-square band-averaged post-fit timing residuals, N_{obs} – the number of observations, N_{ToA} – the number of ToAs, Span – observational data span. See Ref. [39] for details.

Pulsar Name	RMS [μs]	N_{obs}	N_{ToA}	Span [yr]
J0437–4715	0.59	4149	29262	15.0
J1600–3053	0.58	1096	7047	14.2
J1713+0747	0.32	1049	7804	14.2
J1744–1134	0.46	939	6717	14.2
J1909–3744	0.24	2223	14627	14.2
J2241–5236	0.26	821	5224	8.2

We process the data in the same way as Refs. [35, 37]. To extract the target signal from the ToAs, one needs to provide a comprehensive analysis on the noise that might be present in timing residuals. After subtracting the expected arrival times described by the timing model, the timing residuals can be decomposed into

$$\delta t = M\epsilon + \delta t_n + \delta t_s, \quad (13)$$

where $M\epsilon$ accounts for the inaccuracy of the timing model with M being the design matrix and ϵ being the vector of timing model parameter offsets, δt_n contains noise contributions, and δt_s , given by Eq. (12), is the signal that we are searching for.

The noise in all of these pulsars from possible stochastic and deterministic processes has been analyzed by Ref. [40] in great detail. The stochastic noise processes contain white noise and time-correlated red noise. White noise accounts for measurement uncertainties; they are modeled by three parameters EFAC, EQUAD, ECORR [41], with EFAC being the scale factor of ToA uncertainty, EQUAD being an extra component independent of uncertainty and ECORR being the excess variance for sub-banded observations. The red noise includes the spin noise (SN; [42]) from rotational irregularities of the pulsar itself, the dispersion measure variations [43] due to

TABLE II. Parameters and their prior distributions used in the analyses. Here U and log-U represent a uniform and log uniform distribution, respectively. Here “one parameter for PTA” means the parameter is common in the whole data set, while “one parameter per pulsar” indicates the parameter varies from pulsar to pulsar; the same goes for the case of “one parameter per band/system” and “one parameter per exponential-dip event”.

Parameter	description	prior	comments
White noise			
E_k	EFAC per backend/receiver system	U[0, 10]	single-pulsar analysis only
Q_k [s]	EQUAD per backend/receiver system	log-U[−8.5, −5]	single-pulsar analysis only
J_k [s]	ECORR per backend/receiver system	log-U[−8.5, −5]	single-pulsar analysis only
Red noise (including SN and DM)			
\mathcal{A}_{RN}	Red-noise power-law amplitude	log-U[−20, −8]	one parameter per pulsar
γ_{RN}	red-noise power-law index	U[0, 10]	one parameter per pulsar
Band/System noise			
$\mathcal{A}_{\text{BN,GN}}$	band/group-noise power-law amplitude	log-U[−20, −8]	one parameter per band/system
$\gamma_{\text{BN,GN}}$	band/group-noise power-law index	U[0, 10]	one parameter per band/system
Deterministic event			
\mathcal{A}_{E}	exponential-dip amplitude	log-U[−10, −2]	one parameter per exponential-dip event
t_{E} [MJD]	time of the event	U[54500, 54900] for PSR J1713	first exponential-dip event
		U[57500, 57520] for PSR J1713	second exponential-dip event
$\log_{10}\tau_{\text{E}}$ [MJD]	relaxation time for the dip	U[log ₁₀ 5, 2]	one parameter per exponential-dip event
Common noise			
\mathcal{A}_{CN}	common-noise power-law amplitude	log-U[−18, −11]	one parameter for PTA
γ_{CN}	common noise power-law index	U[0, 7]	one parameter for PTA
Ultralight vector dark matter signal			
h_{osc}	oscillation amplitude	log-U[−19, −10] (search) U[−19, −10] (limit)	one parameter for PTA
α_e	oscillation phase on Earth	U[0, 2 π]	one parameter for PTA
α_p	equivalent oscillation phase on pulsar	U[0, 2 π]	one parameter per pulsar
$\cos\theta$	polar angle of propagation direction	U[−1, 1]	one parameter for PTA
ϕ	azimuth angle of propagation direction	U[0, 2 π]	one parameter for PTA
f [Hz]	oscillation frequency	log-U[−9, −7] (search) delta function (limit)	one parameter for PTA fixed
BayesEphem			
z_{drift}	drift-rate of Earth’s orbit about ecliptic z-axis	U[−10 ^{−9} , 10 ^{−9}]	one parameter for PTA
$\Delta M_{\text{jupiter}} [M_{\odot}]$	perturbation to Jupiter’s mass	$\mathcal{N}(0, 1.55 \times 10^{-11})$	one parameter for PTA
$\Delta M_{\text{saturn}} [M_{\odot}]$	perturbation to Saturn’s mass	$\mathcal{N}(0, 8.17 \times 10^{-12})$	one parameter for PTA
$\Delta M_{\text{uranus}} [M_{\odot}]$	perturbation to Uranus’s mass	$\mathcal{N}(0, 5.72 \times 10^{-11})$	one parameter for PTA
$\Delta M_{\text{neptune}} [M_{\odot}]$	perturbation to Neptune’s mass	$\mathcal{N}(0, 7.96 \times 10^{-11})$	one parameter for PTA
PCA_i	principal components of Jupiter’s orbit	U[−0.05, 0.05]	six parameters for PTA

the change in column density of ionized plasma in the interstellar medium, and the band noise (BN) and system (“group”) noise (GN) that are only present in a specific band or system [44]. Red noise is modeled by a power-law spectrum with the amplitude parameter \mathcal{A}_{RN} and spectral index γ_{RN} . In our analysis, we set the number of Fourier frequencies $N_{\text{mode}} = 30$ following Ref. [45] in the calculation of the covariance matrix. For deterministic noise contributions, a typical example is the exponential dip that might be attributed to the sudden change in dispersion in the interstellar medium [43, 44] or change in pulse profile shape [46], and it can be described by an exponential function.

Meanwhile, some systematic errors should be taken into consideration. We use the **BayesEphem** module [47] to account for potential uncertainties in the so-

lar system ephemeris (SSE); we adopt JPL DE438 [48] to project ToAs from the local observatory to the solar system barycenter. Moreover, the North American Nanohertz Observatory for Gravitational Waves (NANOGrav), PPTA, the European Pulsar Timing Array (EPTA), and the International Pulsar Timing Array (IPTA) collaborations all report evidence for an uncorrelated common process (UCP) which can be modeled by a power-law spectrum in their latest data sets [45, 49–51]. Although no definite evidence was found for a Hellings-Downs correlation which is deemed to be necessary for the detection of stochastic gravitational-wave background, the presence of UCP is taken as a promising sign of the gravitational-wave background [45]. Positive Bayesian evidence supporting a scalar-transverse correlation in the process was found in some publications

[52, 53]. However, simulations based on the PPTA DR2 showed that even when no signal is present, the UCP pops out when pulsars have similar intrinsic timing noise [49]. Despite the continuing efforts [54–57], the nature of the UCP remains to be determined, and we hence treat it as a common noise in the analysis.

As Eq. (12) indicates, the vector dark matter signal that we are searching for is described by six parameters: the oscillation amplitude h_{osc} , the oscillation frequency f , the oscillation (propagation) direction described by the polar and azimuth angles (θ, ϕ) and the equivalent phase term in pulsar α_p and in the Earth α_e . In the analyses, we first perform the parameter estimations by including the white noise, red noise, band/system noise, and deterministic noise following [40] for each single pulsar. Then we collect all the chosen pulsars as a whole PTA and allow noise parameters to vary simultaneously with the signal parameters. As the white noise parameters should have little or no correlation with the dark matter parameters, we fix the white noise parameters to their maximum-likelihood values from the single pulsar noise analyses. Fixing white noise parameters should have negligible impact on our results [58] but significantly reduce the computational cost. All the parameters and their priors are listed in Table II.

Similar to the procedure of searching for a gravitational wave background [45, 49], we perform Bayesian inference to extract information from the data. First, we need to determine whether the data \mathcal{D} supports the existence of the signal by calculating the Bayes factor between the noise-plus-signal hypothesis \mathcal{H}_1 and the noise-only hypothesis \mathcal{H}_0 ,

$$\text{BF} = \frac{\Pr(\mathcal{D}|\mathcal{H}_1)}{\Pr(\mathcal{D}|\mathcal{H}_0)}. \quad (14)$$

Here $\Pr(\mathcal{D}|\mathcal{H})$ denotes the evidence given by the integral of the product of the likelihood \mathcal{L} and the prior probability π over the prior volume,

$$\Pr(\mathcal{D}|\mathcal{H}) = \int \mathcal{L}(\mathcal{D}|\Theta)\pi(\Theta)d^n\Theta, \quad (15)$$

where n is the dimension of the parameters Θ . If we do not find significant evidence for the target signal, we place constraints on certain parameters. In the work, we derive the 95% upper limit for the oscillation amplitude \bar{h}_{osc} from its marginal posterior probability distribution,

$$0.95 = \frac{1}{\Pr(\mathcal{D}|\mathcal{H})} \int_0^{\bar{h}_{\text{osc}}} dh_{\text{osc}} \int \mathcal{L}(\mathcal{D}|\Theta)\pi(\Theta)d^{n-1}\Theta', \quad (16)$$

where Θ' denotes all the other parameters except h_{osc} . We use the `enterprise` [59] and `enterprise_extension` [60] packages to evaluate the likelihood and compute the Bayes factor using the product-space method [61–63]. For the Markov-chain Monte-Carlo sampling needed for parameter estimation, we employ the `PTMCMCSampler` package [64].

IV. RESULTS AND DISCUSSION

We first determine whether there is a vector dark matter signal in the data by comparing the signal hypothesis \mathcal{H}_1 and the null hypothesis \mathcal{H}_0 . The log Bayes factor, $\ln \text{BF}$, is about 13.0 for the parameter range $\log_{10}(f/\text{Hz}) \in [-7.2, -7.0]$, seemingly implying strong evidence for a signal. However, when we conduct the search in two separate logarithmic frequency bands $[-9.0, -7.0]$ and $[-7.2, -7.0]$ by excluding PSR J0437–4715, the $\ln \text{BF}$ is found to be 0.5 and 1.5, respectively; these are small Bayes factors that indicates no preference for the signal hypothesis. Therefore, the suspected “signal” is completely due to PSR J0437–4715, and we conclude that it is not a genuine signal. A similar result has been reported in Ref. [37].

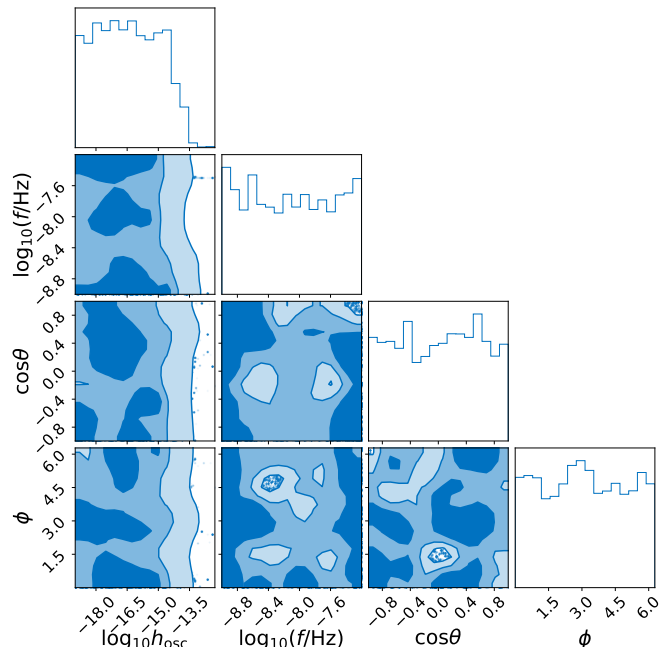


FIG. 1. The posterior distributions for the parameters of the vector dark matter signal, containing the oscillation amplitude h_{osc} , oscillation frequency $\log_{10}(f/\text{Hz}) \in [-9.0, -7.2]$, and the angles of propagation direction θ and ϕ . These posteriors have been marginalized over oscillation phase parameters α_e and α_p .

Fig. 1 shows the posterior distributions of the vector dark matter signal parameters after marginalizing over oscillation phases α_e and α_p . Since we find no evidence of a vector dark matter signal, these posterior distributions resemble those of priors except that we are able to exclude large oscillation amplitudes, i.e., $h_{\text{osc}} \lesssim 10^{-13.5}$. In Fig. 2, we show the 95% upper limits on the oscillation amplitude h_{osc} as a function of frequency. We also plot the predicted amplitude according to Eq. (8) by taking the vector field dark matter density ρ_{VF} equal to the measured local dark matter density $\rho_0 = 0.4 \text{ GeV}/\text{cm}^3$,

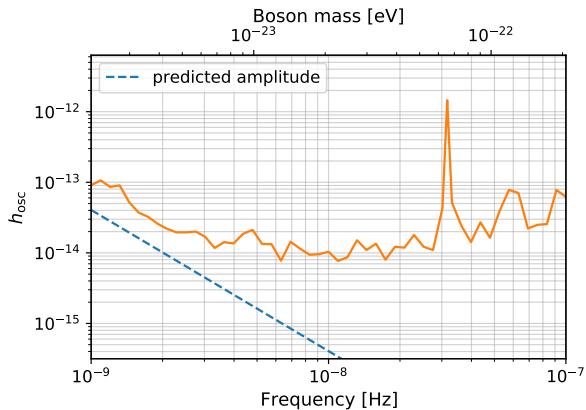


FIG. 2. Upper limits on the signal amplitude h_{osc} (orange line), generated by the vector dark matter in the Galactic as a function of frequency (mass). The blue dashed line shows the model amplitude h_{osc} , assuming $\rho_{\text{VF}} = 0.4 \text{ GeV}/\text{cm}^3$, given by Eq. (8). The peak in the orange curve is due to the loss in sensitivity at the frequency 1 yr^{-1} caused by fitting for the pulsar’s sky location and proper motion [65].

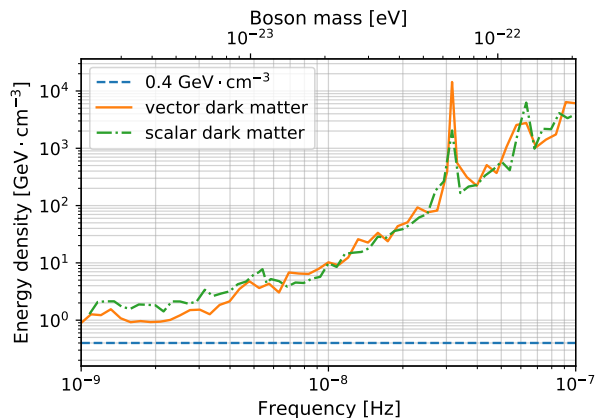


FIG. 3. Upper limits on the vector dark matter density ρ in the vicinity of the Earth (orange line). The green dot-dashed line denotes the upper limits on the scalar dark matter density from PPTA 12-year data set [35] and the blue dashed line denotes the measured dark matter density of $\rho_0 = 0.4 \text{ GeV}/\text{cm}^3$.

assuming that all the dark matter is composed of ultralight vector fields. The predicted amplitude is always below the upper limits, implying we cannot exclude the possibility that the vector fields with masses considered in this work constitute all the dark matter. A more intuitive picture can be obtained by translating the amplitude into the vector field dark matter energy density ρ_{VF} through Eq. (8) and placing the 95% upper limit on the energy density, as shown in Fig. 3. As a comparison, we also plot the upper limits derived from a scalar dark matter search presented in Ref. [35]. We note that the lighter mass provides tighter constraints in our search range. The strongest bound on the dark matter energy density

is $1 \text{ GeV}/\text{cm}^3$ at the lowest frequency 10^{-9} Hz . This is above the local energy density of $\rho_0 = 0.4 \text{ GeV}/\text{cm}^3$, so we cannot place effective constraints on the mass of vector dark matter from current PTA data sets.

The results from this work are consistent with the scalar dark matter search performed with an earlier version of the PPTA data published in 2018. Specifically, our constraints on vector dark matter density $\rho_{\text{VF}} < 5 \text{ GeV}/\text{cm}^3$ for $m \lesssim 10^{-23} \text{ eV}$ is only slightly more stringent than the scalar dark matter density limit of $6 \text{ GeV}/\text{cm}^3$ given by [35]. This is unsurprising because only when the vector field oscillates along a particular direction that is parallel to the line of sight to the pulsar, can we expect the timing residuals induced by the gravitational effect to be three times that caused by the scalar dark matter. However, we do not find a preferred oscillation direction of vector dark matter (see Fig. 1) in the data set.

Several cosmological and astrophysical probes can place constraints on the mass of ultralight dark matter when considering the model has only gravitational coupling. Planck cosmic microwave background data implies a bound on the ultralight dark matter energy density fraction for the $10^{-33} - 10^{-24} \text{ eV}$ mass range [66]. The Lyman- α forest used to trace the underlying dark matter distribution at high redshifts excludes the possibility that the ultralight particles with mass lighter than $2 \times 10^{-20} \text{ eV}$ make up all the dark matter [67]. While the above constraints come from axions and their applicability to ultralight vector dark matter needs to be discussed, the black hole superradiance estimates from supermassive black hole spin measurements constrain the vector dark matter within the mass range $6 \times 10^{-20} - 2 \times 10^{-17} \text{ eV}$ [68]. Although there is no consensus on the constraints on the mass of ultralight dark matter because most of the experiments are subject to their own uncertainties, it is important to note that PTA experiments can constrain the energy density of ultralight dark matter independently and determine whether dark matter is dominated by the ultralight vector particles and thus provide complementary tools to other experiments.

Looking into the future, PTAs based on the Five-hundred-meter Aperture Spherical Telescope [69], MeerKAT [70], and Square Kilometer Array (SKA) [71] with wider frequency bands and large collecting areas, will increase the sensitivity significantly. In the SKA era, a conservative estimate is that 10 years of observations for the 10 best pulsars with an observing cadence of once every 14 days have the potential to constrain the contribution of ultralight dark matter down to 10% of the local dark matter density for $m < 10^{-23} \text{ eV}$ [35]. In the shorter terms sensitivity improvements could be achieved through searches with the IPTA. Combining efforts from PTAs and other experiments will greatly advance our understanding of the nature of dark matter by studying a wide range of dark matter models.

ACKNOWLEDGMENTS

We thank the referee for very useful comments. We acknowledge the use of HPC Cluster of ITP-CAS and HPC Cluster of Tianhe II in National Supercomputing Center in Guangzhou. QGH is supported by the National Key Research and Development Program of China Grant No.2020YFC2201502, grants from NSFC (grant No. 11975019, 11991052, 12047503), Key Research Program of Frontier Sciences, CAS, Grant NO. ZDBS-LY-7009, CAS Project for Young Scientists in Basic Research

YSBR-006, the Key Research Program of the Chinese Academy of Sciences (Grant NO. XDPB15). ZCC is supported by the fellowship of China Postdoctoral Science Foundation No. 2022M710429. RMS acknowledges support through Australian Research Council Future Fellowship FT190100155. This work has been carried out by the Parkes Pulsar Timing Array, which is part of the International Pulsar Timing Array. The Parkes radio telescope (“Murriyang”) is part of the Australia Telescope, which is funded by the Commonwealth Government for operation as a National Facility managed by CSIRO.

-
- [1] V. C. Rubin, Jr. Ford, W. K., and N. Thonnard, “Rotational properties of 21 SC galaxies with a large range of luminosities and radii, from NGC 4605 ($R=4\text{kpc}$) to UGC 2885 ($R=122\text{kpc}$).” *Astrophys. J.* **238**, 471–487 (1980).
 - [2] V. C. Rubin, Jr. Ford, W. K., N. Thonnard, and D. Burstein, “Rotational properties of 23Sb galaxies.” *Astrophys. J.* **261**, 439–456 (1982).
 - [3] S. M. Faber and R. E. Jackson, “Velocity dispersions and mass-to-light ratios for elliptical galaxies.” *Astrophys. J.* **204**, 668–683 (1976).
 - [4] Richard Massey, Thomas Kitching, and Johan Richard, “The dark matter of gravitational lensing,” *Rept. Prog. Phys.* **73**, 086901 (2010), [arXiv:1001.1739 \[astro-ph.CO\]](#).
 - [5] N. Aghanim *et al.* (Planck), “Planck 2018 results. VI. Cosmological parameters,” *Astron. Astrophys.* **641**, A6 (2020), [Erratum: *Astron. Astrophys.* 652, C4 (2021)], [arXiv:1807.06209 \[astro-ph.CO\]](#).
 - [6] Leszek Roszkowski, Enrico Maria Sessolo, and Sebastian Trojanowski, “WIMP dark matter candidates and searches—current status and future prospects,” *Rept. Prog. Phys.* **81**, 066201 (2018), [arXiv:1707.06277 \[hep-ph\]](#).
 - [7] David J. E. Marsh, “Axion Cosmology,” *Phys. Rept.* **643**, 1–79 (2016), [arXiv:1510.07633 \[astro-ph.CO\]](#).
 - [8] Olivier Wantz and E. P. S. Shellard, “Axion Cosmology Revisited,” *Phys. Rev. D* **82**, 123508 (2010), [arXiv:0910.1066 \[astro-ph.CO\]](#).
 - [9] Gianfranco Gentile, P. Salucci, U. Klein, D. Vergani, and P. Kalberla, “The Cored distribution of dark matter in spiral galaxies,” *Mon. Not. Roy. Astron. Soc.* **351**, 903 (2004), [arXiv:astro-ph/0403154](#).
 - [10] W. J. G. de Blok, “The Core-Cusp Problem,” *Adv. Astron.* **2010**, 789293 (2010), [arXiv:0910.3538 \[astro-ph.CO\]](#).
 - [11] B. Moore, S. Ghigna, F. Governato, G. Lake, Thomas R. Quinn, J. Stadel, and P. Tozzi, “Dark matter substructure within galactic halos,” *Astrophys. J. Lett.* **524**, L19–L22 (1999), [arXiv:astro-ph/9907411](#).
 - [12] Anatoly A. Klypin, Andrey V. Kravtsov, Octavio Valenzuela, and Francisco Prada, “Where are the missing Galactic satellites?” *Astrophys. J.* **522**, 82–92 (1999), [arXiv:astro-ph/9901240](#).
 - [13] Marc Schumann, “Direct Detection of WIMP Dark Matter: Concepts and Status,” *J. Phys. G* **46**, 103003 (2019), [arXiv:1903.03026 \[astro-ph.CO\]](#).
 - [14] Paul Bode, Jeremiah P. Ostriker, and Neil Turok, “Halo formation in warm dark matter models,” *Astrophys. J.* **556**, 93–107 (2001), [arXiv:astro-ph/0010389](#).
 - [15] Wayne Hu, Rennan Barkana, and Andrei Gruzinov, “Cold and fuzzy dark matter,” *Phys. Rev. Lett.* **85**, 1158–1161 (2000), [arXiv:astro-ph/0003365](#).
 - [16] Patrick Fox, Aaron Pierce, and Scott D. Thomas, “Probing a QCD string axion with precision cosmological measurements,” (2004), [arXiv:hep-th/0409059](#).
 - [17] Lam Hui, Jeremiah P. Ostriker, Scott Tremaine, and Edward Witten, “Ultralight scalars as cosmological dark matter,” *Phys. Rev. D* **95**, 043541 (2017), [arXiv:1610.08297 \[astro-ph.CO\]](#).
 - [18] Mark Goodsell, Joerg Jaeckel, Javier Redondo, and Andreas Ringwald, “Naturally Light Hidden Photons in LARGE Volume String Compactifications,” *JHEP* **11**, 027 (2009), [arXiv:0909.0515 \[hep-ph\]](#).
 - [19] Ann E. Nelson and Jakub Scholtz, “Dark Light, Dark Matter and the Misalignment Mechanism,” *Phys. Rev. D* **84**, 103501 (2011), [arXiv:1105.2812 \[hep-ph\]](#).
 - [20] Kazunori Nakayama, “Vector Coherent Oscillation Dark Matter,” *JCAP* **10**, 019 (2019), [arXiv:1907.06243 \[hep-ph\]](#).
 - [21] Peter W. Graham, Jeremy Mardon, and Surjeet Rajendran, “Vector Dark Matter from Inflationary Fluctuations,” *Phys. Rev. D* **93**, 103520 (2016), [arXiv:1504.02102 \[hep-ph\]](#).
 - [22] Kimihiro Nomura, Asuka Ito, and Jiro Soda, “Pulsar timing residual induced by ultralight vector dark matter,” *Eur. Phys. J. C* **80**, 419 (2020), [arXiv:1912.10210 \[gr-qc\]](#).
 - [23] Andrew J. Long and Lian-Tao Wang, “Dark Photon Dark Matter from a Network of Cosmic Strings,” *Phys. Rev. D* **99**, 063529 (2019), [arXiv:1901.03312 \[hep-ph\]](#).
 - [24] Peter W. Graham, David E. Kaplan, Jeremy Mardon, Surjeet Rajendran, and William A. Terrano, “Dark Matter Direct Detection with Accelerometers,” *Phys. Rev. D* **93**, 075029 (2016), [arXiv:1512.06165 \[hep-ph\]](#).
 - [25] Aaron Pierce, Keith Riles, and Yue Zhao, “Searching for Dark Photon Dark Matter with Gravitational Wave Detectors,” *Phys. Rev. Lett.* **121**, 061102 (2018), [arXiv:1801.10161 \[hep-ph\]](#).
 - [26] R. Abbott *et al.* (LIGO Scientific Collaboration, Virgo Collaboration,, KAGRA, Virgo), “Constraints on dark photon dark matter using data from LIGO’s and Virgo’s third observing run,” *Phys. Rev. D* **105**, 063030 (2022), [arXiv:2105.13085 \[astro-ph.CO\]](#).
 - [27] Diego Blas, Diana Lopez Nacir, and Sergey Sibiryakov,

- “Ultralight Dark Matter Resonates with Binary Pulsars,” *Phys. Rev. Lett.* **118**, 261102 (2017), [arXiv:1612.06789 \[hep-ph\]](#).
- [28] Diana López Nacir and Federico R. Urban, “Vector Fuzzy Dark Matter, Fifth Forces, and Binary Pulsars,” *JCAP* **10**, 044 (2018), [arXiv:1807.10491 \[astro-ph.CO\]](#).
- [29] D. Antypas *et al.*, “New Horizons: Scalar and Vector Ultralight Dark Matter,” (2022), [arXiv:2203.14915 \[hep-ex\]](#).
- [30] Andrei Khmelnitsky and Valery Rubakov, “Pulsar timing signal from ultralight scalar dark matter,” *JCAP* **02**, 019 (2014), [arXiv:1309.5888 \[astro-ph.CO\]](#).
- [31] M. V. Sazhin, “Opportunities for detecting ultralong gravitational waves,” *Soviet Ast.* **22**, 36–38 (1978).
- [32] Steven L. Detweiler, “Pulsar timing measurements and the search for gravitational waves,” *Astrophys. J.* **234**, 1100–1104 (1979).
- [33] R. S. Foster and D. C. Backer, “Constructing a Pulsar Timing Array,” *Astrophys. J.* **361**, 300 (1990).
- [34] N. K. Porayko and K. A. Postnov, “Constraints on ultralight scalar dark matter from pulsar timing,” *Phys. Rev. D* **90**, 062008 (2014), [arXiv:1408.4670 \[astro-ph.CO\]](#).
- [35] Nataliya K. Porayko *et al.*, “Parkes Pulsar Timing Array constraints on ultralight scalar-field dark matter,” *Phys. Rev. D* **98**, 102002 (2018), [arXiv:1810.03227 \[astro-ph.CO\]](#).
- [36] Ryo Kato and Jiro Soda, “Search for ultralight scalar dark matter with NANOGrav pulsar timing arrays,” *JCAP* **09**, 036 (2020), [arXiv:1904.09143 \[astro-ph.HE\]](#).
- [37] Xiao Xue *et al.* (PPTA), “High-precision search for dark photon dark matter with the Parkes Pulsar Timing Array,” *Phys. Rev. Res.* **4**, L012022 (2022), [arXiv:2112.07687 \[hep-ph\]](#).
- [38] P. Salucci, F. Nesti, G. Gentile, and C. F. Martins, “The dark matter density at the Sun’s location,” *Astron. Astrophys.* **523**, A83 (2010), [arXiv:1003.3101 \[astro-ph.GA\]](#).
- [39] Matthew Kerr *et al.*, “The Parkes Pulsar Timing Array project: second data release,” *Publ. Astron. Soc. Austral.* **37**, e020 (2020), [arXiv:2003.09780 \[astro-ph.IM\]](#).
- [40] Boris Goncharov *et al.*, “Identifying and mitigating noise sources in precision pulsar timing data sets,” *Mon. Not. Roy. Astron. Soc.* **502**, 478–493 (2021), [arXiv:2010.06109 \[astro-ph.HE\]](#).
- [41] Zaven Arzoumanian *et al.* (NANOGrav), “The NANOGrav Nine-year Data Set: Observations, Arrival Time Measurements, and Analysis of 37 Millisecond Pulsars,” *Astrophys. J.* **813**, 65 (2015), [arXiv:1505.07540 \[astro-ph.IM\]](#).
- [42] Ryan M. Shannon and James M. Cordes, “Assessing the Role of Spin Noise in the Precision Timing of Millisecond Pulsars,” *Astrophys. J.* **725**, 1607–1619 (2010), [arXiv:1010.4794 \[astro-ph.SR\]](#).
- [43] M. J. Keith *et al.*, “Measurement and correction of variations in interstellar dispersion in high-precision pulsar timing,” *Mon. Not. Roy. Astron. Soc.* **429**, 2161 (2013), [arXiv:1211.5887 \[astro-ph.GA\]](#).
- [44] L. Lentati *et al.*, “From Spin Noise to Systematics: Stochastic Processes in the First International Pulsar Timing Array Data Release,” *Mon. Not. Roy. Astron. Soc.* **458**, 2161–2187 (2016), [arXiv:1602.05570 \[astro-ph.IM\]](#).
- [45] Zaven Arzoumanian *et al.* (NANOGrav), “The NANOGrav 12.5 yr Data Set: Search for an Isotropic Stochastic Gravitational-wave Background,” *Astrophys. J. Lett.* **905**, L34 (2020), [arXiv:2009.04496 \[astro-ph.HE\]](#).
- [46] R. M. Shannon *et al.*, “The Disturbance of a Millisecond Pulsar Magnetosphere,” *Ap.J.L.* **828**, L1 (2016), [arXiv:1608.02163 \[astro-ph.HE\]](#).
- [47] M. Vallisneri *et al.* (NANOGrav), “Modeling the uncertainties of solar-system ephemerides for robust gravitational-wave searches with pulsar timing arrays,” *Astrophys. J.* **893**, 112 (2020), [arXiv:2001.00595 \[astro-ph.HE\]](#).
- [48] William M. Folkner and Ryan S. Park, “Planetary ephemeris DE438 for Juno,” Tech. Rep. IOM392R-18-004, Jet Propulsion Laboratory, Pasadena, CA (2018).
- [49] Boris Goncharov *et al.*, “On the evidence for a common-spectrum process in the search for the nanohertz gravitational-wave background with the Parkes Pulsar Timing Array,” *The Astrophys. J. Lett.* **917**, L19 (2021), [arXiv:2107.12112 \[astro-ph.HE\]](#).
- [50] J. Antoniadis *et al.*, “The International Pulsar Timing Array second data release: Search for an isotropic gravitational wave background,” *Mon. Not. Roy. Astron. Soc.* **510**, 4873–4887 (2022), [arXiv:2201.03980 \[astro-ph.HE\]](#).
- [51] S. Chen *et al.*, “Common-red-signal analysis with 24-yr high-precision timing of the European Pulsar Timing Array: inferences in the stochastic gravitational-wave background search,” *Mon. Not. Roy. Astron. Soc.* **508**, 4970–4993 (2021), [arXiv:2110.13184 \[astro-ph.HE\]](#).
- [52] Zu-Cheng Chen, Yu-Mei Wu, and Qing-Guo Huang, “Searching for Isotropic Stochastic Gravitational-Wave Background in the International Pulsar Timing Array Second Data Release,” (2021), [arXiv:2109.00296 \[astro-ph.CO\]](#).
- [53] Zu-Cheng Chen, Chen Yuan, and Qing-Guo Huang, “Non-tensorial gravitational wave background in NANOGrav 12.5-year data set,” *Sci. China Phys. Mech. Astron.* **64**, 120412 (2021), [arXiv:2101.06869 \[astro-ph.CO\]](#).
- [54] Xiao Xue *et al.*, “Constraining Cosmological Phase Transitions with the Parkes Pulsar Timing Array,” *Phys. Rev. Lett.* **127**, 251303 (2021), [arXiv:2110.03096 \[astro-ph.CO\]](#).
- [55] Yu-Mei Wu, Zu-Cheng Chen, and Qing-Guo Huang, “Constraining the Polarization of Gravitational Waves with the Parkes Pulsar Timing Array Second Data Release,” *Astrophys. J.* **925**, 37 (2022), [arXiv:2108.10518 \[astro-ph.CO\]](#).
- [56] Zu-Cheng Chen, Yu-Mei Wu, and Qing-Guo Huang, “Search for the Gravitational-wave Background from Cosmic Strings with the Parkes Pulsar Timing Array Second Data Release,” *Astrophys. J.* **936**, 20 (2022), [arXiv:2205.07194 \[astro-ph.CO\]](#).
- [57] Ligong Bian, Jing Shu, Bo Wang, Qiang Yuan, and Junchao Zong, “Searching for cosmic string induced stochastic gravitational wave background with the Parkes Pulsar Timing Array,” (2022), [arXiv:2205.07293 \[hep-ph\]](#).
- [58] Z. Arzoumanian *et al.* (NANOGrav), “The NANOGrav 11-year Data Set: Pulsar-timing Constraints On The Stochastic Gravitational-wave Background,” *Astrophys. J.* **859**, 47 (2018), [arXiv:1801.02617 \[astro-ph.HE\]](#).
- [59] Justin A. Ellis, Michele Vallisneri, Stephen R. Taylor, and Paul T. Baker, “Enterprise: Enhanced numerical toolbox enabling a robust pulsar inference suite,” Zenodo (2020).

- [60] Stephen R. Taylor, Paul T. Baker, Jeffrey S. Hazboun, Joseph Simon, and Sarah J. Vigeland, “[enterprise_extensions](#),” (2021), v2.2.0.
- [61] Bradley P. Carlin and Siddhartha Chib, “Bayesian model choice via markov chain monte carlo methods,” *Journal of the Royal Statistical Society. Series B (Methodological)* **57**, 473–484 (1995).
- [62] Sonke Hee, Will Handley, Mike P. Hobson, and Anthony N. Lasenby, “Bayesian model selection without evidences: application to the dark energy equation-of-state,” *Mon. Not. Roy. Astron. Soc.* **455**, 2461–2473 (2016), [arXiv:1506.09024 \[astro-ph.CO\]](#).
- [63] Stephen R. Taylor, Rutger van Haasteren, and Alberto Sesana, “From Bright Binaries To Bumpy Backgrounds: Mapping Realistic Gravitational Wave Skies With Pulsar-Timing Arrays,” *Phys. Rev. D* **102**, 084039 (2020), [arXiv:2006.04810 \[astro-ph.IM\]](#).
- [64] Justin Ellis and Rutger van Haasteren, “[jellis18/ptmcmcsampler: Official release](#),” (2017).
- [65] X. J. Zhu *et al.*, “An all-sky search for continuous gravitational waves in the Parkes Pulsar Timing Array data set,” *Mon. Not. Roy. Astron. Soc.* **444**, 3709–3720 (2014), [arXiv:1408.5129 \[astro-ph.GA\]](#).
- [66] Renée Hlozek, David J. E. Marsh, and Daniel Grin, “Using the Full Power of the Cosmic Microwave Background to Probe Axion Dark Matter,” *Mon. Not. Roy. Astron. Soc.* **476**, 3063–3085 (2018), [arXiv:1708.05681 \[astro-ph.CO\]](#).
- [67] Keir K. Rogers and Hiranya V. Peiris, “Strong Bound on Canonical Ultralight Axion Dark Matter from the Lyman-Alpha Forest,” *Phys. Rev. Lett.* **126**, 071302 (2021), [arXiv:2007.12705 \[astro-ph.CO\]](#).
- [68] Masha Baryakhtar, Robert Lasenby, and Mae Teo, “Black Hole Superradiance Signatures of Ultralight Vectors,” *Phys. Rev. D* **96**, 035019 (2017), [arXiv:1704.05081 \[hep-ph\]](#).
- [69] Rendong Nan, Di Li, Chengjin Jin, Qiming Wang, Lichun Zhu, Wenbai Zhu, Haiyan Zhang, Youling Yue, and Lei Qian, “The Five-Hundred-Meter Aperture Spherical Radio Telescope (FAST) Project,” *Int. J. Mod. Phys. D* **20**, 989–1024 (2011), [arXiv:1105.3794 \[astro-ph.IM\]](#).
- [70] M. Bailes *et al.*, “The MeerKAT telescope as a pulsar facility: System verification and early science results from MeerTime,” *Publ. Astro. Soc. Aust.* **37**, e028 (2020), [arXiv:2005.14366 \[astro-ph.IM\]](#).
- [71] T J W Lazio, “The square kilometre array pulsar timing array,” *Classical and Quantum Gravity* **30**, 224011 (2013).